*Bangladesh Journal of Physics, Vol. **27**, Issue 2, pp. 27–37, 2020*

CRYSTAL STRUCTURE REFINEMENT, MAGNETIC AND MÖSSBAUER ANALYSIS OF $LaFeO_3$ PEROVSKITE SYNTHESIZED BY SOL-GEL METHOD

S. M. AL IMRAN HOSSAIN[1*], M. K. ROLY[2], T. M. IMRAN[1]

[1]*Department of Physics, Jagannath University, Dhaka-1100, Bangladesh*

[2]*Scientific Information Division, Bangladesh Atomic Energy Commission, Dhaka 1207, Bangladesh*

**Corresponding author e-mail: smalimran.hossain@phy.jnu.ac.bd*

Received on 26.06.2020, Revised received on 24.09.2020, Accepted for publication on 01.10.2020

DOI: https://doi.org/10.3329/bjphy.v27i2.57664

ABSTRACT

In this present study, $LaFeO_3$ nanoparticles have been successfully synthesized by sol-gel method and annealed the produced sample at 600 °C, 800 °C, 1000 °C, 1200 °C. The influence of annealing temperature on the structural, morphological and magnetic properties of the developed nanoparticles has been investigated systematically. The XRD patterns confirmed the absence of impurity or secondary phase in the spectra. Orthorhombic crystal system of *pbnm* space group was successfully determined by Rietveld refinement. Scherrer method was used to calculate crystallite size. An increasing trend in crystallite size and improving crystallinity were obtained with increasing annealing temperature. Scanning Electron Microscopy (SEM) images showed a homogeneous distribution of increasing average particle sizes ranging from 35 nm to 450 nm. Magnetic hysteresis (M-H) loop was recorded at room temperature revealed weak ferromagnetism in nanocrystalline lanthanum ferrite. The maximum magnetization was found to be 1.82 emu/g at 600 °C, and it was sharply decreased to 0.33 emu/g at 1200 °C annealing temperature. Interactions between the antiferromagnetic and ferromagnetic exchange coupling are influenced by the uncompensated spin canting causes to accomplish the ordering of weak ferromagnetism in $LaFeO_3$. Moreover, the bond length of Fe-O and the bond angle of Fe-O-Fe were decreased with decreasing annealing temperature. As a result, Fe ions, come closer to each other, enhancing the ferromagnetic exchange interaction between iron ions via oxygen ions made significant contributions to the magnetic properties of $LaFeO_3$ nanoparticles. Mössbauer spectroscopy was used to find the nature of interactions for the observed magnetic behavior depending on different site environments with varying annealing temperatures.

Keywords: *Perovskite, Rietveld refinement, Bond-Angle, Magnetization, Mössbauer Spectroscopy*

1. INTRODUCTION

At present, it is a common practice to create new functional materials and enhance the performance of existing complex oxide because of their attractive properties. In the case of effective material properties and improving functionality, composite interfaces play a vital role [1]. Enhancement of the properties of functional materials rudimentarily happens because of the interaction between two interfaces [2]. Several phenomena occur at the interface such as rearrangement of chemical bonding [3], spin-charge and orbital reconstruction [4], electronic structure modifications [5] etc. There are several types of complex oxide functional materials such as some are magnetic insulators; some possess strong covalent bonds with antiferromagnetic metals while some are responsive at the presence of an external magnetic field.

Among those functional materials, Perovskite rare-earth based ferrites of the type ABO_3 (where A is a rare earth element and B is a 3*d* transition metal) are very promising due to their innovative use in advance technologies [6]. They have attracted significant attention for various types of applications in solid oxide fuel cells [7], chemical sensors [8], magnetic materials [9, 10], thermoelectric [11] and oxygen permeation membranes [12, 13]. Continuous study of past years has shown that physical properties of a perovskite composite mainly influenced by its rare-earth

atoms. On the other hand, transition metal plays a central role to change the electric and magnetic properties of its ground state. These perovskites have partially filled 3*d* bands and yet are magnetic insulators. A potential gap is eventually introduced due to strong Coulomb interaction between these insulators which is not attenuated in this narrow band. The insulating gap solely depends on the constituent atoms that make up the solid. One can named this gap either the Mott-Hubbard intraband *d*-*d* type or the charge transfer (CT) intraband *p*-*d* type [14]. The magnetic properties of these types of strongly correlated electron systems can be manipulated by the suitable annealing temperature in order to change particle size from nano level to bulk structure and get various interesting properties, such as transitions may happen from antiferromagnetism to ferromagnetism or antiferromagnetism to paramagnetism.

Among various types of perovskites, $LaFeO_3$ (LFO) is one of the most common perovskite type oxides that has an orthorhombic structure with *pbnm* space group [15]. Bulk LFO is antiferromagnetic with a very high Neel temperature of 740K while its spontaneous magnetization is considerably small, $0.44\mu_B$/Fe [16]. However, it is a common phenomenon for antiferromagnetic nanoparticles to show increasing net magnetization results from uncompensated surface spins [17, 18]. If it is possible to promote ferromagnetic nature in LFO, it will surely provide lots of technological applications with the help of its customized magnetic field. Magnetic properties of well-defined LFO perovskite are still notable to investigate. Normally, LFO nanoparticles can be prepared by various methods such as electrospinning [19], hydrothermal [20], microwave-assisted method [21], sonochemical method [22], sol-gel [23, 24] and polymerization complex method [25, 26]. Among these above-mentioned methods, Sol-gel method is widely used in all over the world because it enables better composition control and chemical homogeneity of the final products [27, 28].

In this work, the synthesis of LFO nanoparticles was performed via citric sol-gel method. The relation among crystallite size, structural parameters (specifically bond angle and bond length, cell volume, etc.), magnetization, and relative area of different ion sites of LFO perovskite as a function of temperature were investigated. In view of these, we investigated the crystal structure, magnetic hysteresis loop, and Mössbauer spectroscopy of the LFO perovskite.

2. EXPERIMENTAL

LFO powders were synthesized by citric sol-gel method. Analytical grade of La $(NO_3)_3.6H_2O$, Fe $(NO_3)_3.9H_2O$, citric acid (CA) and ethylene glycol (EG) were used as raw materials. Firstly, La $(NO_3)_3.6H_2O$, Fe $(NO_3)_3.9H_2O$ and citric acid (CA) at molar ratio of 1:1:2 were dissolved in a mixture of 200 ml deionized water, then stirred for 5 min on a hot plate magnetic stirrer, followed by the addition of 10 ml ethylene glycol to the mixture with continuous stirring. After the addition, the temperature was raised to 80 °C under constant stirring of 650 rpm. Another 10 ml of ethylene glycol was added when the remaining mixture was approximately 100 ml. The complex precursor was stirred until a sol was formed and finally cooled down to room temperature. Then the sol was dried for 24 hours at 120 °C to remove the liquid content and to produce a gelled mass. The gel was then ground in an agate mortar until homogenous powders were formed. Then a programmable furnace was used for annealing the prepared powders at heating rate 5 °C/min at different temperatures (600 °C, 800 °C, 1000 °C & 1200 °C) for 3 hours in. For avoiding the cracking of the samples, all the samples were subjected to cool down naturally inside the furnace. The annealed powders were then ground again for 30 minutes to obtain the pure phase of LFO. Phase and structure of the products were investigated by XRD (PANalytical Empyrean) with CuK_α

radiation (λ = 1.54056 Å). Field emission scanning electron microscope (FESEM) (model: JEOL, JSM-7600F) was employed to observe the surface morphology of LFO powder samples. The magnetization vs. applied magnetic field (M-H) hysteresis loops of the samples were investigated using a Vibrating Sample Magnetometer (VSM, Model EV-9 MicroSense LLC, USA). The magnetic parameters including coercivity (H_c), saturation magnetization (M_s), and remanent magnetization (M_r), were obtained from this measurement. Mössbauer spectroscopy with a model of VT400 was used to acquire Mössbauer spectra operated in constant acceleration mode in transmission geometry at room temperature. The source employed was ^{57}Co in Rh matrix of strength 50 mCi. The Mössbauer spectra were analyzed by using a WMOSS 4R software with the IR (intermediate relaxation) module.

3. RESULTS AND DISCUSSION

3.1 Structural and Morphological Analysis

Figure 1 represents the XRD patterns of LFO annealing at different temperatures that are 600 °C, 800 °C, 1000 °C and 1200 °C for 3 hours. All the samples have shown sharp and well-defined peaks with orthorhombic crystal structure having no impurity phase and LFO endorses the stabilization of perovskite phase. Low-intensity characteristic peaks of perovskite phase appeared, as soon as the sample was annealed at 600 °C. It was seen that crystallinity of the LFO was improved with increasing temperature. Because further heating only increased the intensity of the X-ray peaks and no other peaks were observed. The crystallite size can be determined from Debye-Scherrer's equation:

$$D = \frac{k\lambda}{\beta cos\theta}$$

Where, D is the crystallite size, θ is the Bragg angle, λ is the wavelength of the X-ray radiation; β is the full width at half maximum height (FWHM) of the diffraction peak located at 2θ, the constant k is taken as 0.9 [29].

The values of the particle size, crystallite size and FWHM for the annealed samples are reported in Table 1. The crystallite size of LFO sample annealed at 600 °C is 20 nm which is smaller than 28 nm for LFO sample annealed at 800 °C. Similarly, the crystallite size is 39 nm for the sample annealed at 1000°C, apparently smaller than 50 nm annealed at 1200 °C. Hence, it is a clear indication of the crystallite size effect on the annealing temperature of these ferrites.

Table 1: Particle size, crystallite size and FWHM for different annealing temperatures of LFO samples.

Temperatures (°C)	Particle Size (nm)	Crystallite Size (nm)	FWHM (Deg.)
600	35	20	0.4265
800	70	28	0.3132
1000	170	39	0.2232
1200	450	50	0.178

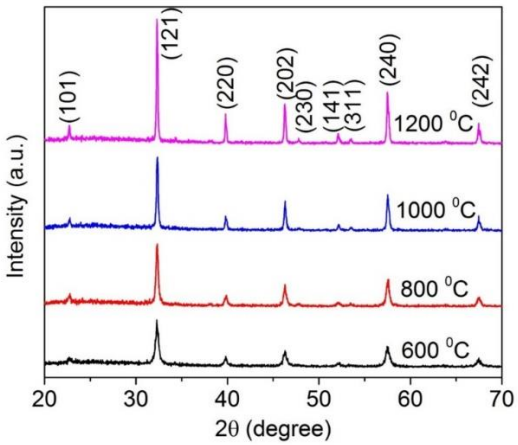

Fig. 1: XRD patterns of LFO nanoparticles annealed at different annealing temperatures (600 °C - 1200 °C) for 3 hours.

The lattice parameters, cell volumes, Fe-O bond lengths, Fe-O-Fe bond angles and densities of LFO samples were estimated from the Rietveld's method. In Fig. 2, Rietveld's refinement of X-ray data was performed by using *FullProf suite Program* ver. 6.00 [30]. However, in the Rietveld method, the Pseudo-Voigt function, which is a linear combination of both the Gaussian (crystallite size) and the Lorentzian (microstrains) functions, was used to fit the peak's shape profile. It can be seen that the calculated lattice parameters are in good agreement with those of the orthorhombic phase of LFO [31] and found to remain constant throughout the inspection of varying annealing temperatures. However, the cell volume increased with increasing bond length and decreased with increasing bond angle. This is due to fact that, contribution of increasing bond angle compensated more to the effect of increasing bond length. Hence, we have a slight increase in cell volume with increasing annealing temperature. The values of other parameters such as profile residual (R_p), weighted profile (R_{wp}) and quality factor for goodness-of-fitting (GOF) (χ^2) obtained after iterative refinement cycles are also reported in Table 2.

Another investigation was carried out by FESEM analysis to show the surface morphology of the synthesized particles, as well as the development of grain structure. Figure 3 displays FESEM micrographs (magnification ×100,000) which show the effect of annealing temperature on the microstructure of LFO nanoparticles. The calculated average particle sizes of samples using Image J are tabulated in Table 1. It shows a clear increasing trend in particle size with increasing annealing temperatures. At 600 °C, the powder has irregular microstructure with a small particle size of about 35 nm. However, at 800 °C, spherical shaped particles were found. However, particles were agglomerated, so the size was slightly bigger than the previous one. On the other hand, when the temperature was raised to 1000 °C that spherical shape was almost disappeared. Instead, we have found relatively bigger particles of 170 nm indicated that this temperature, 1000 °C, is sufficient for the start of crystal growth. The clear and homogeneous microstructure becomes more pronounced for the sample annealed at 1200 °C as shown in Fig. 3.

Now, if we see the Table 1, we can find that particle size is relatively larger than crystallite size in all annealing temperatures used in the present work. The reason is that during the synthesis, crystallites make agglomeration to each other and eventually end up with a larger particle size.

Particle agglomerations are governed by several dominating factors such as particle shape, surface area, porosity and density etc. [32].

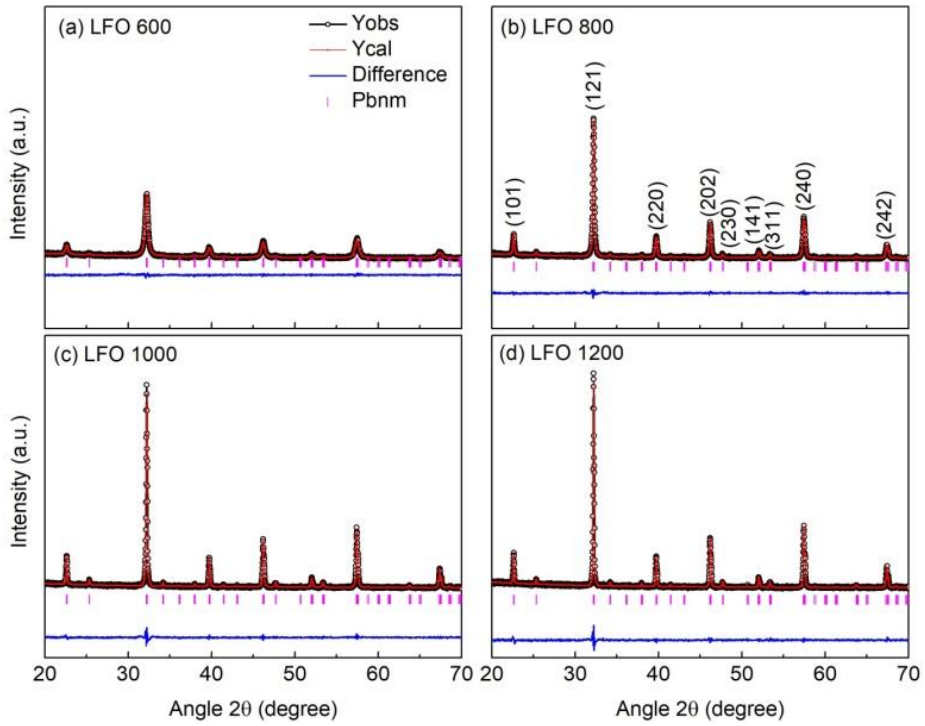

Fig. 2: Rietveld refined XRD pattern of LFO samples annealed at 600 °C, 800 °C, 1000 °C and 1200 °C respectively.

Table 2: Structural parameters obtained from Rietveld refinement of X-ray diffraction pattern for LFO samples annealed at different temperatures.

Sample	Lattice Parameters (Å)	Cell Volume ($Å^3$)	Fe-O length (Å)	Fe-O-Fe angle (Deg.)	Density (g/cm^3)	Factors (%)
LFO 600 °C	a = 5.55 b = 5.56 c = 7.84	242.47	1.88	154.35	5.43	R_P = 34.7 R_{wp} = 21.3 χ^2 = 1.16
LFO 800 °C	a = 5.55 b = 5.56 c = 7.84	242.41	1.94	157.19	5.97	R_P = 29.1 R_{wp} = 17.4 χ^2 = 1.15
LFO 1000 °C	a = 5.55 b = 5.56 c = 7.84	242.33	1.95	157.95	6.12	R_P = 33.5 R_{wp} = 19.9 χ^2 = 1.61
LFO 1200 °C	a = 5.55 b = 5.56 c = 7.84	242.28	1.97	158.37	6.25	R_P = 39.3 R_{wp} = 21.6 χ^2 = 1.83

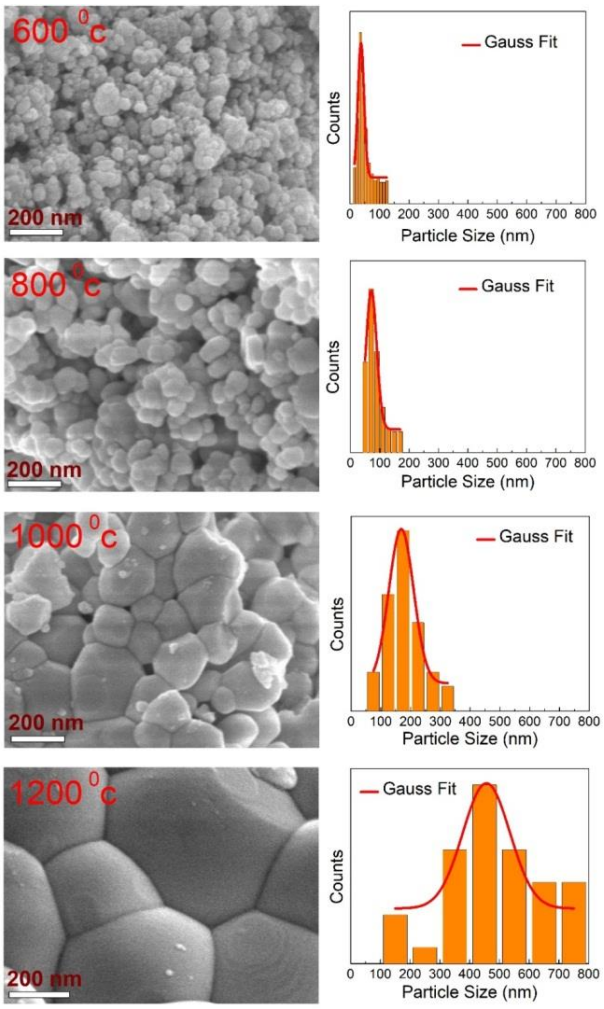

Fig. 3: FESEM micrographs of the produced LFO nanoparticles annealed at 600 °C, 800 °C, 1000 °C and 1200 °C respectively.

3.2 Magnetic Properties

To explore the magnetic properties, the field-dependent magnetic hysteresis loops of the synthesized nanoparticles were investigated with an applied magnetic field of up to ±10 KOe are shown in Fig. 4. Table 3 gives a synopsis of the resulting saturation magnetization (M_s), remnant magnetization (M_r) and coercivity (H_c) as a function of annealing temperature of the produced samples. It was reported in a number of previous investigations that the magnetic spins in lanthanum ferrite materials systems are ordered antiferromagnetically [33, 34]. The saturation magnetization (M_s) and the remnant magnetization were decreased (M_r) with the increasing annealing temperature. It can be observed from the hysteresis loops that at 600 ^{0}C, the saturation magnetization reached a maximum value of 1.82 emu/g compared to that of the other samples.

Afterwards, the value gradually declined with the increase in annealing temperature, and eventually, at 1200 ^{0}C it plunged to a low value of 0.33 emu/g.

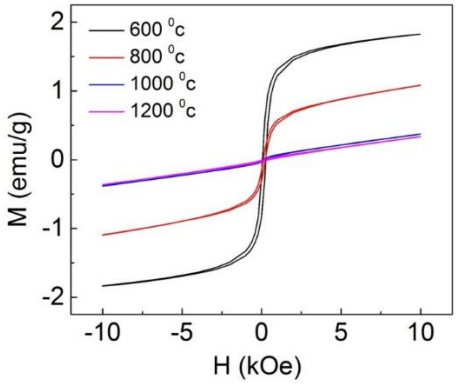

Fig. 4: Effect of annealing temperature on M-H hysteresis loop of LFO nanoparticles synthesized by sol-gel method.

Table 3: Saturation magnetization (M_s), remanent magnetization (M_r) and coercive field (H_c) of LFO nanoparticles annealed at 600, 800, 1000 and 1200 °C respectively.

Sample	M_s (emu/g)	M_r (emu/g)	H_c (Oe)
LFO 600 °C	1.83	0.3006	150.87
LFO 800 °C	1.08	0.0709	388.96
LFO 1000 °C	0.37	0.0119	352.24
LFO 1200 °C	0.33	0.0114	158.18

To reveal the underlying cause of higher value of magnetization at lower annealing temperature, we did several inspections on particle size, crystallite size, Fe-O-Fe bond angle and Fe-O bond length that can liberate the spins from the canted cycloid structure. The weak ferromagnetic behavior of the LFO nanoparticles can be attributed firstly to the distorted spins from the surface causing canted spins of Fe moments [35, 36]. The uncompensated spins on the exterior surface make a ferromagnetic shield over the antiferromagnetic interior of the particles, which in turn produces a nonzero magnetization. The decrease of particle size corresponds to the increased number of unsaturated spins [37]. Another possible reason to enhance the ferromagnetic behavior is the double exchange (DE) interaction of Fe^{3+}-O^{2-}-Fe^{4+} between neighboring Fe^{3+} and Fe^{4+} ions [38]. Therefore, at lower annealing temperatures, the smaller particles have more uncompensated spins on the surface and experience stronger DE interaction than the bigger ones. As a result, the weak ferromagnetic ordering is induced in the synthesized nanoparticles and hence, the magnetization gets increased. On the other hand, the results for 1000 ˚C and 1200 ˚C also demonstrated that, although a few amounts of locked spins are liberated due to the rotation of the FeO_6 octahedron, the intrinsic antiferromagnetic interaction occurs strongly in the bulk like particles [39, 40]. Moreover, due to the bond length of Fe-O and the bond angle of Fe-O-Fe are increased with increasing annealing temperature, the Fe ions stay further to each other causing the

exchange interaction becomes reduced. Also, the larger particle sizes correspond to a lesser number of unsaturated spins on the surface. Hence the samples at higher annealing temperatures show weaker ferromagnetic behavior. The effect of annealing temperature on crystallite size and saturation magnetization is shown in Fig. 5.

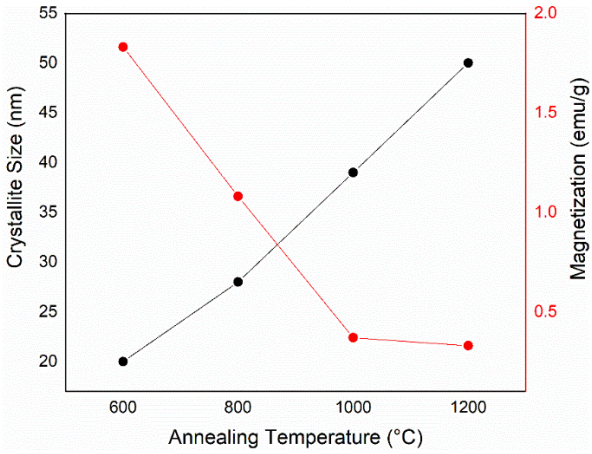

Fig. 5: Variation of crystallite size and saturation magnetization as a function of annealing temperature.

3.3 Mössbauer Analysis

To investigate the identification of magnetic field distribution for the magnetic behavior in LFO samples, room temperature Mössbauer spectra were studied. Figure 6 shows the Mössbauer spectra of the LFO samples which have sextet patterns with Mössbauer parameters shown in Table 4. Mössbauer spectra from Fe ions have shown one or a set of doublets with particular values of isomer shift and quadruple splitting on both A or B sites of the samples. Approximate value of isomer shift is 0.37 ± 0.01 mm/s for A site while it is 0.40 ± 0.03 mm/s for B site atom. It is obvious due to the larger relative area of B site than the A site in the LFO perovskite system. Moreover, isomer shift values may indicate that the S-electron charge distribution of Fe^{3+} ions change with La substitution. So, during the de-excitation of a nucleus it is possible to increase or decrease the effective nuclear size as it does not have a sharp boundary. Therefore, size effect of nucleus may reduce the interaction energy and hence the variation of isomer shift occurs. These values of isomer shift confirm the presence of Fe is in the +3 oxidation states [41].

Table 4: Hyperfine parameters deconvoluted from Mössbauer spectrum for $LaFeO_3$ nanoparticles annealed at different temperature.

Sample (°C)	**Isomer Shift (δ) (mm/s)**		**Quadruple splitting (ΔEq) (mm/s)**		**Hyperfine field (H_{int}) (kG)**		**Relative Area (R_A) (%)**	
Site	A	B	A	B	A	B	A	B
600	0.36	0.37	0.47	0.46	520.7	489.7	0.30	0.70
800	0.37	0.42	1.36	0.15	525.23	499.46	0.11	0.89
1000	0.37	0.44	1.19	0.17	525.06	502.89	0.12	0.88
1200	0.37	0.43	0.15	0.05	525.10	509.16	0.14	0.86

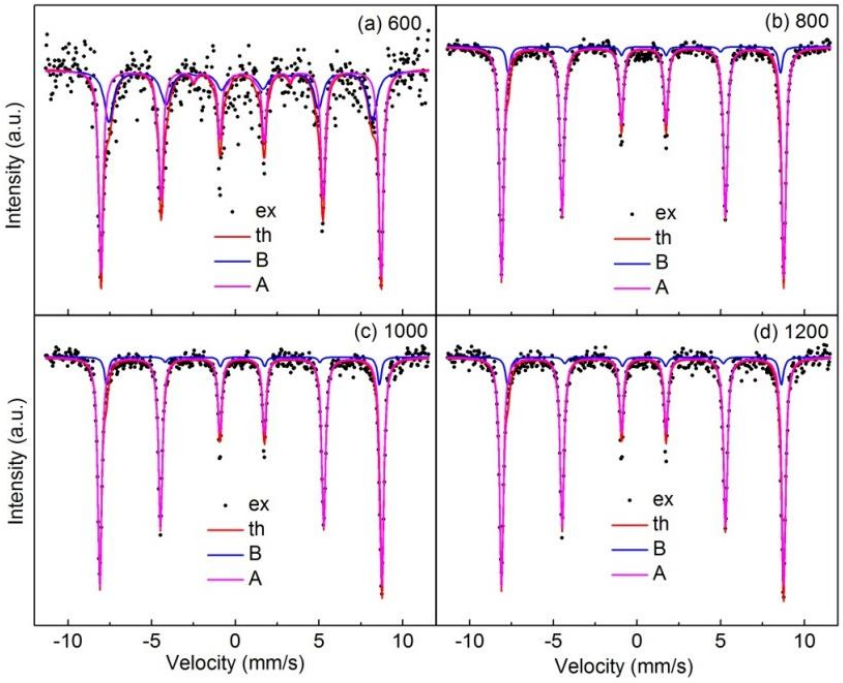

Fig. 6: Mössbauer spectra of $LaFeO_3$ samples annealed at 600°C, 800°C, 1000°C and 1200°C respectively.

From Table 4 it can be observed that the relative area of B site is 0.70 while A site is 0.30 for annealing temperature of 600°C. There is a drastic decrease of the relative area of A site for the annealing temperature of ≥ 800°C. This demonstrates that at low temperature annealing, presence of higher relative area value of A site gives rise to the greater number of ferromagnetic couplings between A and B sites leading to the uncompensated parallel spin. Thus, the magnetization presented in Fig. 4 is higher for this sample. However, for the annealing temperature of 800°C and above the area of A site becomes smaller leading to the significant amount of compensated unparalleled spin on B site which eventually gives rise to the smaller value of magnetization. Again, the quadrupole splitting at A site jumps to a higher value of 1.36 mm/s accompanied by the increasing temperature started from 600°C. Though, the quadrupole splitting at B site reduces when annealing temperature is increased. The increase in bond angle Fe-O-Fe may cause the reduction in the electric field gradient at the nuclei. Also, from Table 4, it is observed that the hyperfine field (H_{int}) is slightly increased with increasing annealing temperature at B site, while at A site it does not change appreciably. This little increase may be attributed to the increase in Fe-O bond length. Since O^{2-} is a weak field ligand, which gives rise to the high spin state of the Fe ion. Those electrons in *3d* orbitals cause the observed increase in hyperfine field strength. Since, the hyperfine field has greater tendency to stabilize at higher annealing temperature indicating that the bond length of Fe-O tends to stabilize. Therefore, magnetically ordered Fe ions produce the sextet patterns with six absorption lines reflecting hyperfine magnetic splitting and the line widths are often sensitive to LFO samples' crystallinity and annealing temperature.

4. CONCLUSIONS

This investigation illustrated that variation in annealing temperature played a remarkable role on structural parameters, particle size and magnetic properties of LFO powder samples synthesized by sol-gel method. XRD patterns and their refined extrapolated data revealed that crystallinity and other structural parameters of the prepared samples changed significantly with the change in annealing temperature, also confirmed from particle size obtained from SEM investigations. The room temperature weak ferromagnetism was confirmed from the VSM analysis for the prepared nanoparticles of lower annealing temperatures. This could be due to the fact that, the magnetic moment of LFO nanoparticles originated from the spin uncompensation at the surface. As the particle size decreases, an increasing fraction of atoms lie at or near the surface and then the spin uncompensation increases. Hence, the moment of an antiferromagnetic particle is expected to increase significantly with decreasing particle size. The Mössbauer spectra support the findings in magnetization and are consistent with a diluted exchange coupling between Fe^{3+} ions in A and B sites are determined from the ratios of the area under two sublattices with respect to La content.

ACKNOWLEDGEMENTS

We are thankful to Materials science division, Bangladesh Atomic Energy Center, Dhaka, Bangladesh for recording VSM and Mössbauer measurements. We are also grateful to the Department of Chemistry, Jagannath University, Dhaka, Bangladesh.

REFERENCES

[1] J. Zhou, L.L Liu, Q. Zhang, P. Li, Schi. technol. Adv. Mater **13 (**2012), 045001.

[2] Q. Zhan., R. Yu, H. Zheng, C.R. Kisielowski, R. Ramesh, Appl. Phys. Lett. **89** (2006) 172902.

[3] A.P. Sutton., R.W. Balluffi, (Clarendon, Oxford), pp. 149-239, (1995).

[4] R. Ramesh, Current Sci. **105** (2013) 1107-1114.

[5] S. Pillai, D. Bhuwal, D. Banerjee, A. Shelke, Appl. Phys. Lett. **102** (2013) 072907.

[6] W.Y. Lee, H. J. Yun, J.W. Yoon, Journal of alloys and compounds **583**, (2014) 320.

[7] S. Phokha, S. Pinitsoontorn, S. Rujirawat and S. Maensiri, Physica B **55**, (2015) 476.

[8] S. M. Khetre, A. U. Chopade, C. J. Khilare, S. R. Kulal, H. V. Jadhav, P. N. Jagadale, S. V. Bangale and S. R, Bamane, Journal of Shivaji Uni. (Sci. & Tech.) **41(2**) (2014) 250.

[9] D. Wang, M. Gong, J. Appl. Phys. **109** (2011) 114304.

[10] T. J. Park, G.C. Papaefthymiou, A. J. Viescas, A.R. Moodenbaugh, S. S. Wong, Nano Lett. **7** (2007) 766.

[11] D. L. Minh, H. Mai, N. Dinh, N. Ngoc, T. Thuy, and J. Vnu, Mathematics Physics **29(3)**, (2013) 42.

[12] H. J. M. Bouwmeester, A. J. Buggraaf, Membr. Sci. Technol. **4**, (1996) 435.

[13] A. L. Shaula, V. V. Kharton, N. P. Vyshakto, E. V. Tsipis, M. V. Patrakeev, F. M. B. Marques and J. R. Frade, J.Eur. Ceram. Soc. **25(4)** (2005) 489.

[14] J. B. Torrance, P. Lacorre, C. Asavaroengchai and R. Metzger, J. Solid State Chem. **90** (1991) 168.

[15] S. Geller, E. A. Wood, Acta. Cryst. **9**, (1956) 563.

[16] D. Treves, J. Appl. Phys. **36** (1965) 1033.

[17] R. H. Kodama, A. E. Berkowitz, Phys. Rev. B **59** (1999) 6321.

[18] Y. C. Lee, A. B. Parkhomov, K. M. Krishnan, J. Appl. Phys. **107** (2010) 09E124.

[19] S. Li, X. Wang, Optik. **126** (2015) 408.

[20] H. Xiao, C. Xue, P. Song, P. Li and Q. Wang, Appl. Surf. Sci. **337**, (2015) 65.

[21] P. Tang, Y. Tong, H. Chen H, F. Cao and G. Pan, Appl. Phys. **13** (2013) 340.

[22] M. Sivakumar, A. Gedanken, W. Zhong, Y. Jiang and, I. Brukental, D. Bhattacharya Y. Yeshurun and I. Nowik, J. Mater. Chem. **14** (2004) 764.

[23] S. B. Kansara, D. Dhruv, D. D. Joshi, S. Pandy, P. S. Rayaprol, D. G. Solanki and N. A. Kuberkar, Appl. Surf. Sci. **356**, (2015) 1272.

[24] T. Liu, Y. Xu, Materials Chemistry and Physics **129** (2011) 1047.

[25] Z. Yang, Y. Huang, B. Dong, H. L. Li, Materials Research Bulletin **41**, (2006) 274.

[26] Y. Janbutrach, S. Hunpratub, S. Swatsitang, Nanoscale Res. Lett. **9** (2014) 498.

[27] M. Mohammadi, S. Baghshahi, A. Ghasemi, Journal of Materials Science: Materials in Electronics **27** (2016) 11447.

[28] S. A. Sayyed, Ebrahimi, J. Non-Cryst. Solids **353** (2016) 802.

[29] A. M. Badr, H. A. Elshaikh and H. H. Afify, Journal of Phy. D: Applied Phys. **50** (2017) 505111.

[30] P. Jangade, P. R. Arjunwadkar and M. A. Nagarbawadi, Journal of Applied Phys. **8(6)** (2016) 57-60.

[31] S. Hunpratub, A. Karaphun, S. Phokha and E. Swatsitang, Appl. Surf. Sci. **380** (2016) 52.

[32] M. Salavati-Niasari, F. Davar, T. Mahmoudi, Polyhedron **28**, (2009) 1455.

[33] M. M. Hessien, A. El-Maghraby, M. M. Rashad, Mater. Technol.: Adv. Perform. Mater **30** (2015) 70.

[34] E. Swatsitang, A. Karaphun, S. Phokha, S. Hunpratub and T. Putjuso, J. Sol-Gel Sci. Technol **81** (2017) 483.

[35] N.T. Thuy, D.L. Minh, Adv. Mater. Sci. Eng. **2012** (2012) 6.

[36] Y. Qiu, Y. S. Luo, Z. J. Zou, Z. M. Tian, S. L. Yuan, Y. Xi, L. Z. Huang, J. Mater. Sci.: Mater. Electron. **25** (2013) 760.

[37] E. Cao, Y. Zhang, W. Hao and H. Peng, Materials Letters **190** (2017) 143.

[38] S. Phokha, S. Pinitsoontorn, S. Maensiri, S. Rujirawat, J. Sol-Gel Sci. Technol. **71**(2014) 333.

[39] F. Huang, Z. Wang, X. Lu, J. Zhang, K. Min, W. Lin, R. Ti, T. Xu, J. He, C. Jue and J. Zhu, Sci. Rep. **3** (2013) 2907.

[40] T. J. Park, G. C. Papaehymiou, A. J. Viescas, A. R. Moodenbaugh and S. S. Wong, Nano Lett. **7** (2007) 766.

[41] M. Sorescu, T. Xu, J. D. Burnett, J. A. Aitken, Journal of Materials Science: Materials in Electronics, **46** (2011) 6709.